Supporting Information

Pd loading threshold for an efficient noble metal use in Pd/CeO_2 methane oxidation catalysts

Deniz Zengel[1], Vasyl Marchuk[1], Merve Kurt[1], Florian Maurer[1], Agustin Salcedo[2], Carine Michel[2], David Loffreda[2], Mimoun Aouine[3], Stephane Loridant[3], Philippe Vernoux[3], Heike Störmer[4], Maria Casapu[1*], Jan-Dierk Grunwaldt[1,5*]

[1]Institute for Chemical Technology and Polymer Chemistry (ITCP), Karlsruhe Institute of Technology (KIT), Kaiserstr. 12, 76131 Karlsruhe, Germany

[2]ENSL, CNRS, Laboratoire de Chimie UMR 5182, 46 allée d'Italie, F69364 Lyon, France

[3]Univ Lyon, Université Claude Bernard-Lyon 1, CNRS, IRCELYON-UMR 5256, 2 av. A. Einstein, F-69626 Villeurbanne Cedex, France

[4]Laboratory for Electron Microscopy (LEM), Karlsruhe Institute of Technology (KIT), 76131 Karlsruhe, Germany

[5] Institute of Catalysis Research and Technology (IKFT), Karlsruhe Institute of Technology (KIT), Hermann-von-Helmholtz-Platz 1, 76344 Eggenstein-Leopoldshafen, Germany

* Corresponding authors:

Jan-Dierk Grunwaldt, Institute for Chemical Technology and Polymer Chemistry (ITCP), Karlsruhe Institute of Technology (KIT), Kaiserstr. 12, 76131 Karlsruhe, Germany, Tel.: +49 721 608 42120

Maria Casapu, Institute for Chemical Technology and Polymer Chemistry (ITCP), Karlsruhe Institute of Technology (KIT), Kaiserstr. 12, 76131 Karlsruhe, Germany, Tel.: +49 721 608 43192

E-mail: grunwaldt@kit.edu; maria.casapu@kit.edu

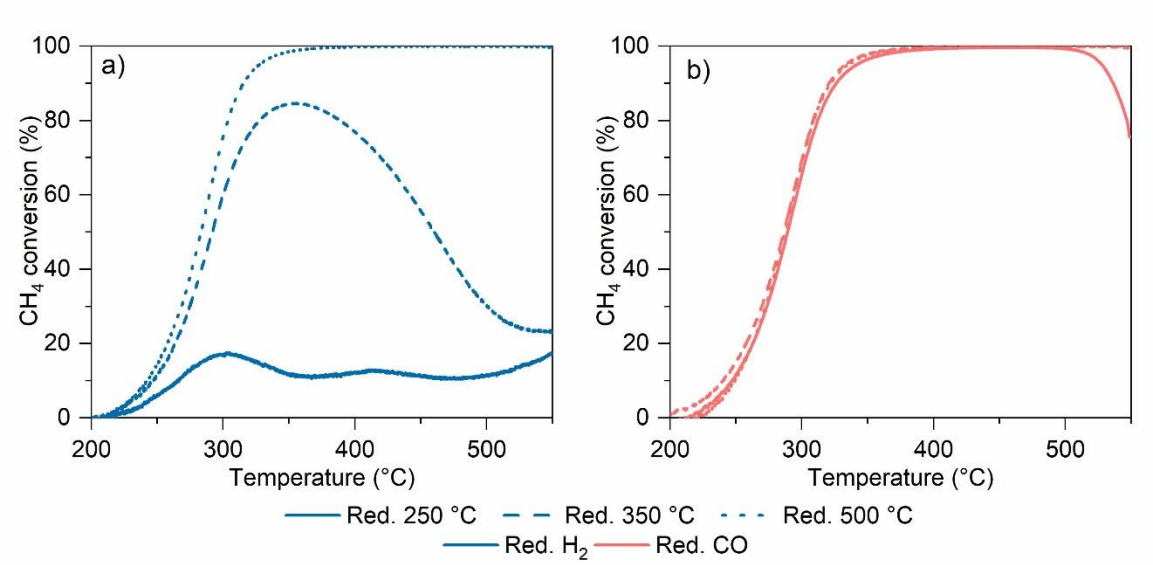

Figure S1. Conversion of methane by total oxidation during 1st light-off for 1%Pd/CeO_2-120 after reduction for 1 h in 2% H_2/N_2 at 250 °C, 350 °C and 500 °C (a), and in 0.5% CO/N_2 at 250 °C, 350 °C and 500 °C (b). Gas mixture: 3200 ppm CH_4, 10 vol.% O_2 in N_2 at a weight hourly space velocity of 20000 $L \cdot g_{NM}^{-1} \cdot h^{-1}$.

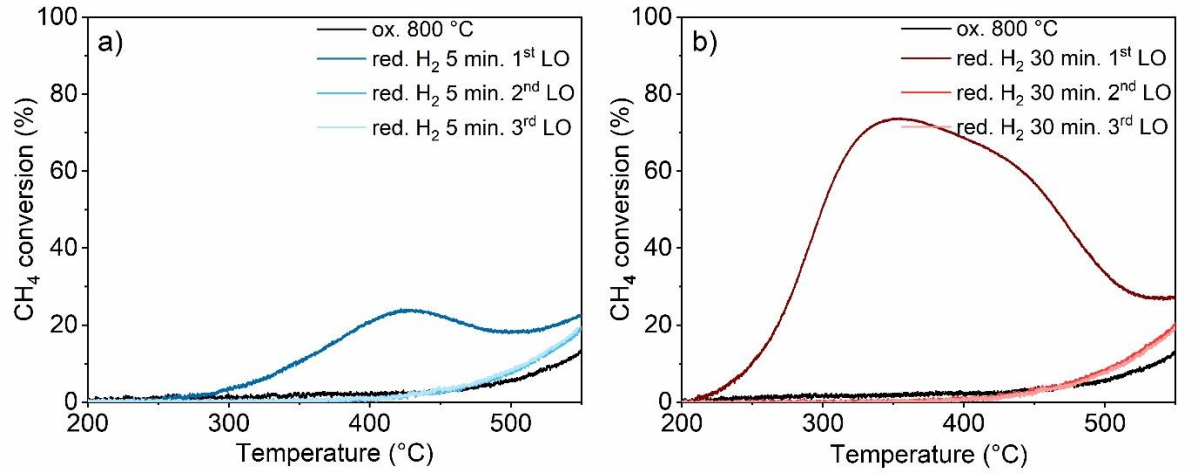

Figure S2. Conversion of methane by total oxidation during 1st, 2nd and 3rd light-offs for 2 wt.% Pd/CeO_2-120 after oxidation at 800 °C for 1 h and reduction for 5 min (a) and 30 min (b) in 2 % H_2/N_2 at 500 °C. Gas mixture: 3200 ppm CH_4, 10 vol.% O_2 in N_2 at a weight hourly space velocity of 20000 $L \cdot g_{NM}^{-1} \cdot h^{-1}$.

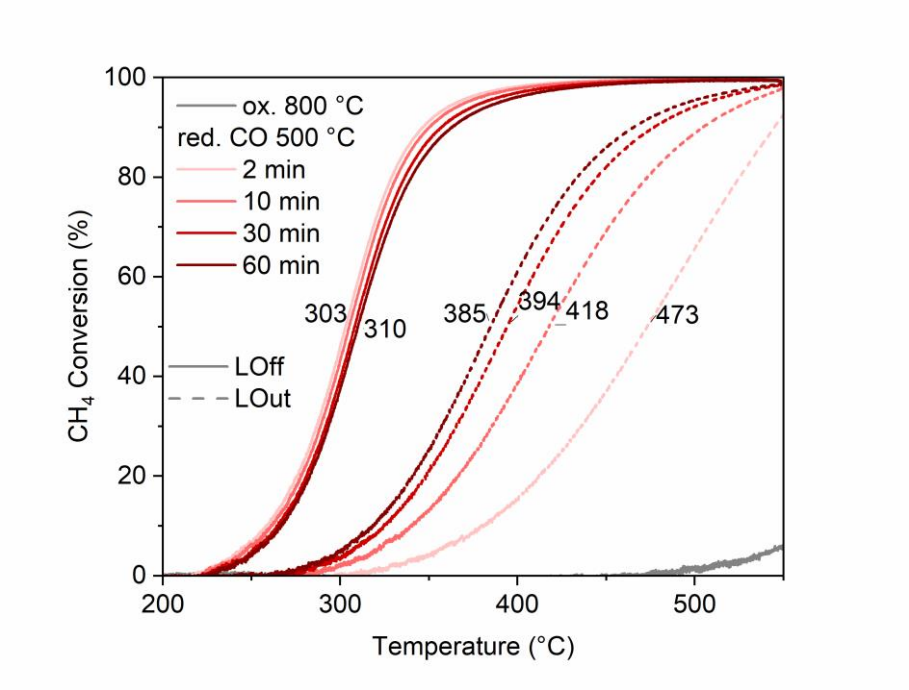

Figure S3. Conversion of methane by total oxidation during light-off (full line) and light-out (dotted lines) for 2 wt.% Pd/CeO_2-120 after oxidation at 800 °C for 1 h and reduction for 2-60 min in 0.5% CO/N_2 at 500 °C. Gas mixture: 3200 ppm CH_4, 10 vol.% O_2 in N_2 at a weight hourly space velocity of 20000 $L \cdot g_{NM}^{-1} \cdot h^{-1}$.

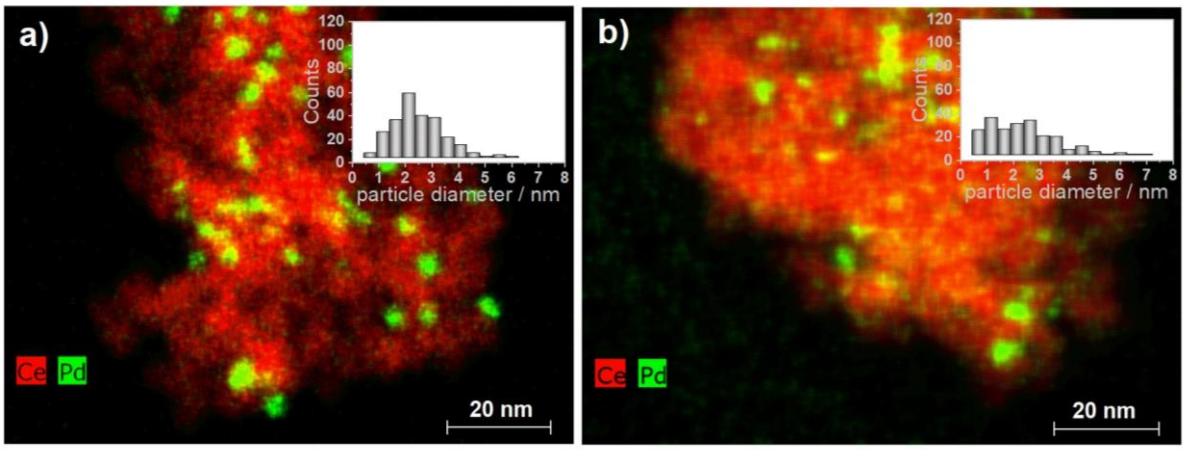

Figure S4. HAADF-STEM EDXS images and particle size distribution for 2 wt.% Pd/CeO_2-120 catalyst after CO reductive treatment at 500 °C for 1 h (a) and after 3 light-off/light-out cycles (b).

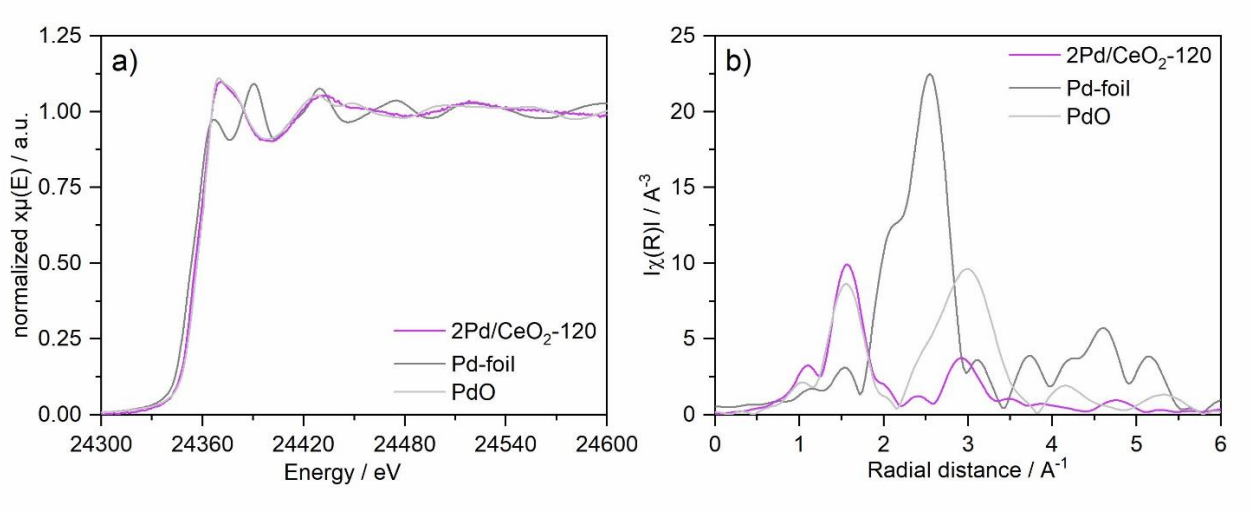

Figure S5. XANES (a) and FT-EXAFS (b) spectra collected at Pd K edge for the 2 wt.% Pd/CeO_2-120 after degreening at 800 °C for 10 h in static air.

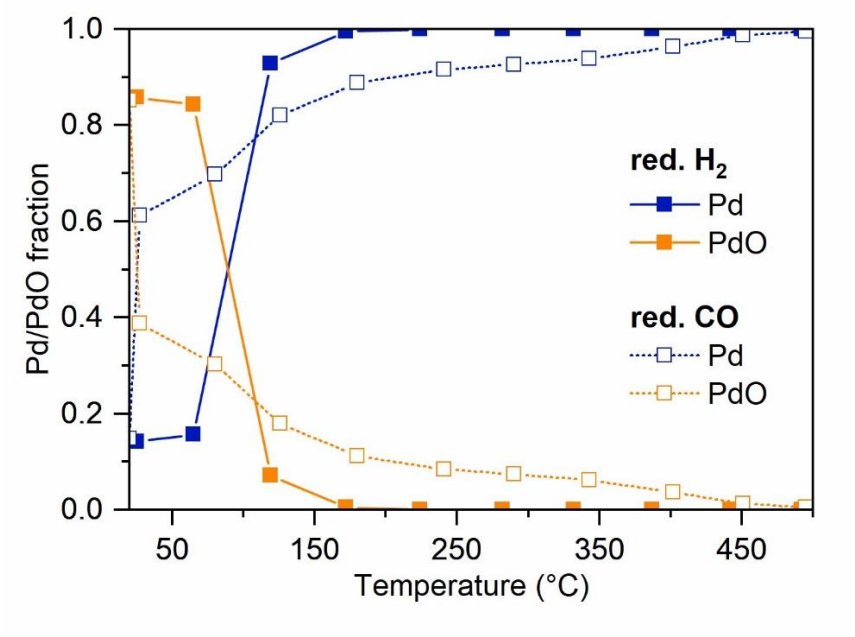

Figure S6. Results of linear combination fitting of the XANES region (-20 eV to 30 eV around the edge) during H_2 reduction and CO reduction using the catalyst degreened at 800°C for 10 h in static air as Pd^{2+}(PdO-like) state and the catalyst reduced in H_2 at 500°C as Pd^0 state.

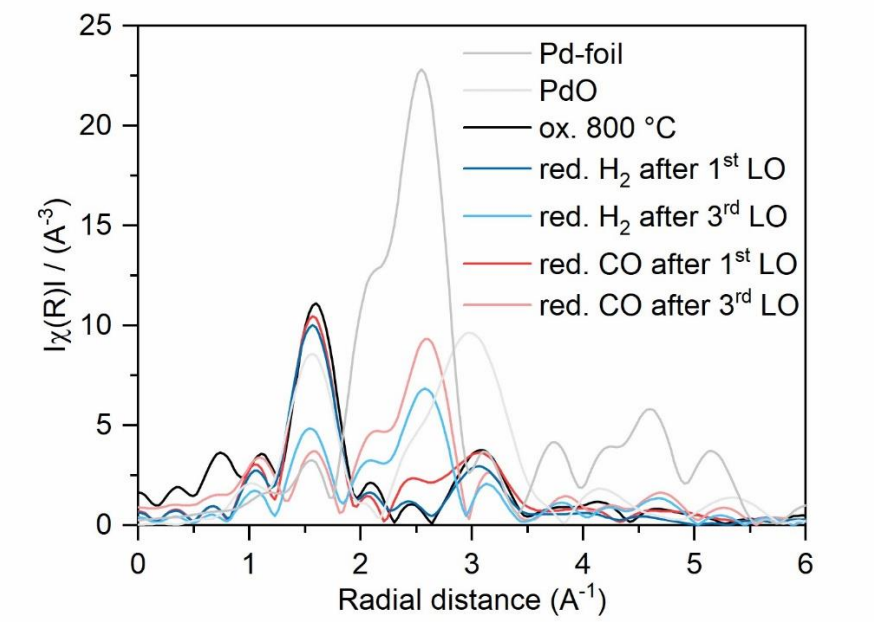

Figure S7. k^3-weighted FT-EXAFS spectra collected at Pd K edge for the 2 wt.% Pd/CeO_2-120 after degreening at 800 °C for 10 h in static air, activation by reduction with CO and H_2, and after 3 light-off/light-out CH_4 oxidation cycles.

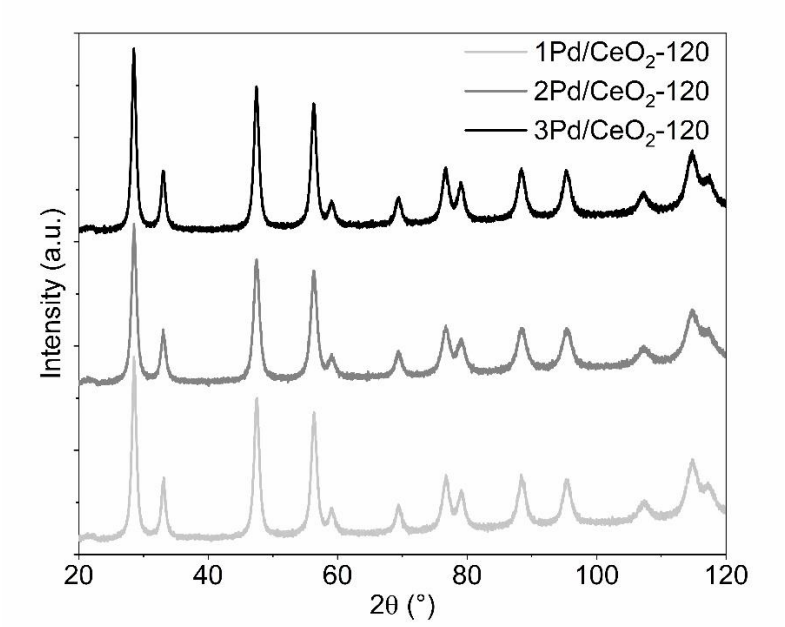

Figure S8. X-ray diffractograms of the prepared Pd/CeO_2-120 samples, all reflections are due to ceria, no detectable reflections of PdO or Pd over a range of 2Θ = 20-120°.

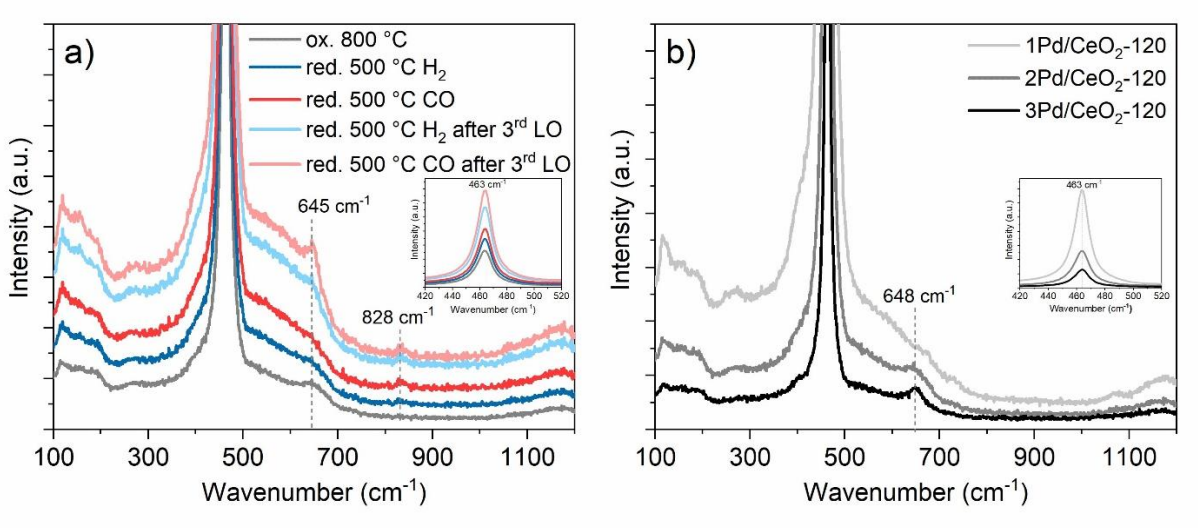

Figure S9. Raman spectra of the CeO_2-120 supported catalysts. (a) 2 wt.% Pd/CeO_2-120 sample after different treatments. (b) Differently loaded Pd/CeO_2-120 catalysts after calcination at 800 °C for 10 h.

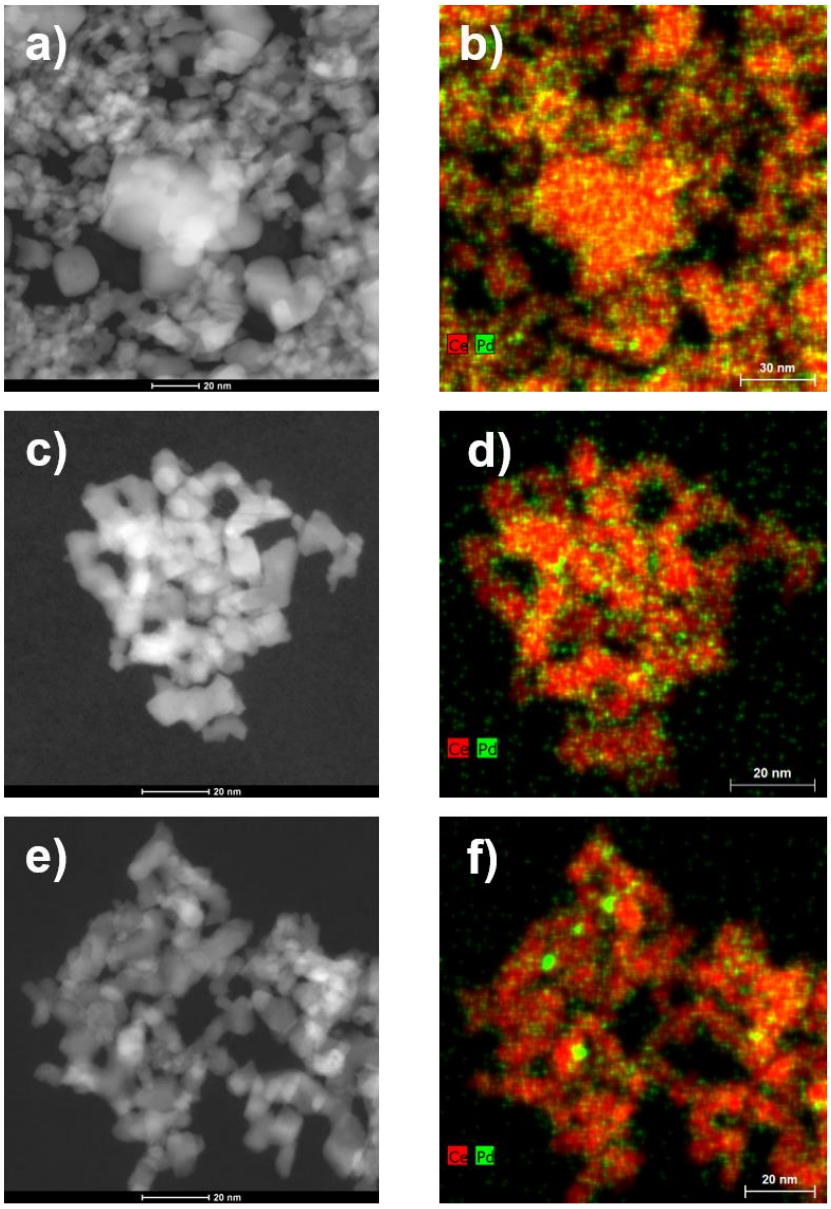

Figure S10. TEM images (left) and EDXS-maps (right) of 1 wt.% Pd/CeO_2-120 (a + b), 2 wt.% Pd/CeO_2-120 (c + d) and 3 wt.% Pd/CeO_2-120 (e + f) after calcination at 800 °C for 10 h.

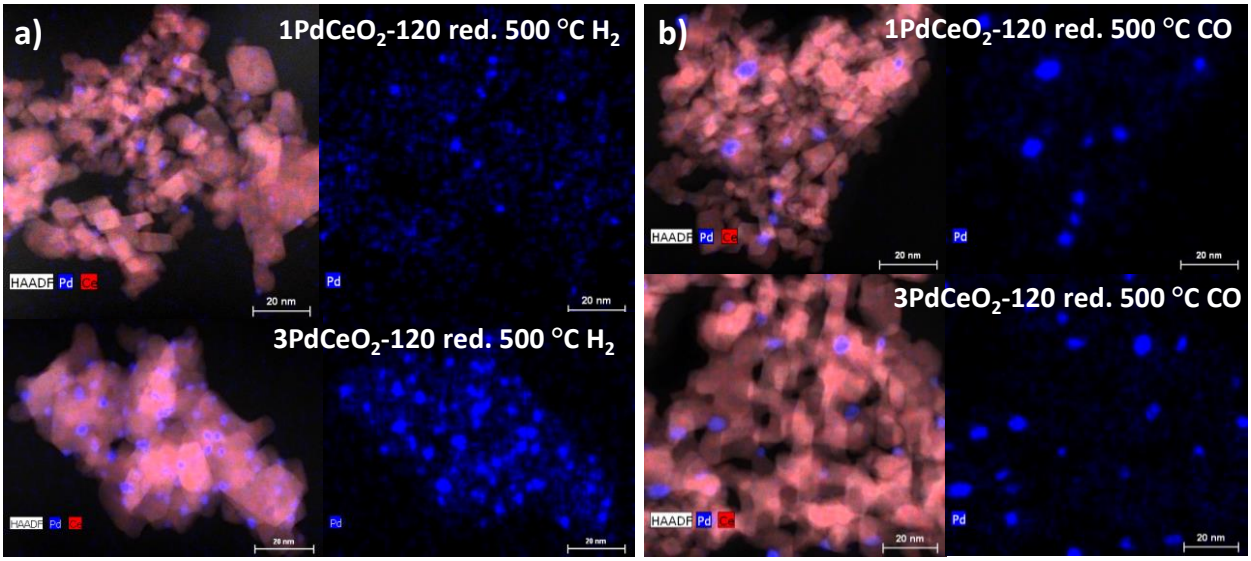

Figure S11. EDXS-maps of 1 wt.% Pd/CeO_2-120 (top) and 3 wt.-% Pd/CeO_2-120 (bottom) reduction in 2 % H_2/N_2 (a) or in 2 % CO/N_2 (b) at 500 °C for 1 h.

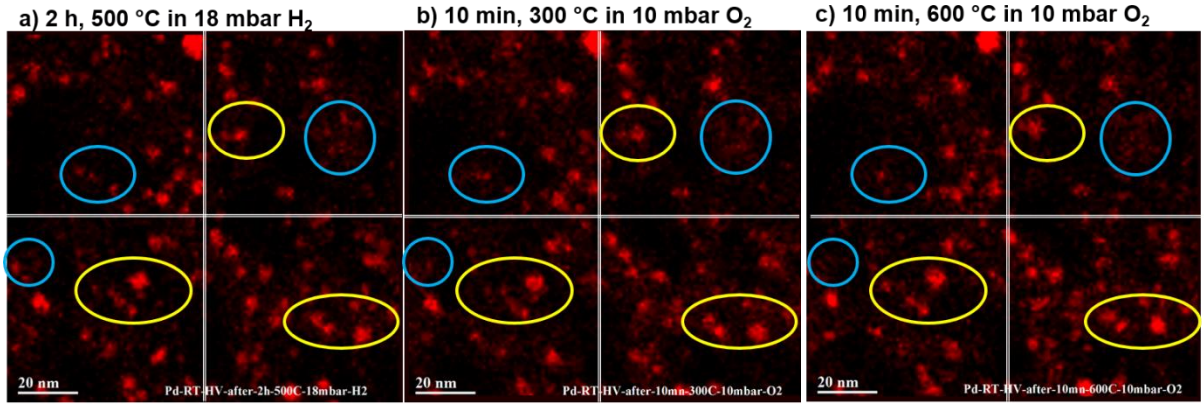

Figure S12. EDXS-maps of 3 wt.% Pd/CeO_2-120 during different treatment procedures. Small nanoparticles (< 5 nm) located in regions with a low noble metal surface concentration are completely redispersed under oxidizing conditions (marked with blue circles). Larger particles but also small nanoparticles located at regions with high noble metal surface concentration are only partially redispersed and appear flatten during exposure to oxygen (regions marked with yellow circles).

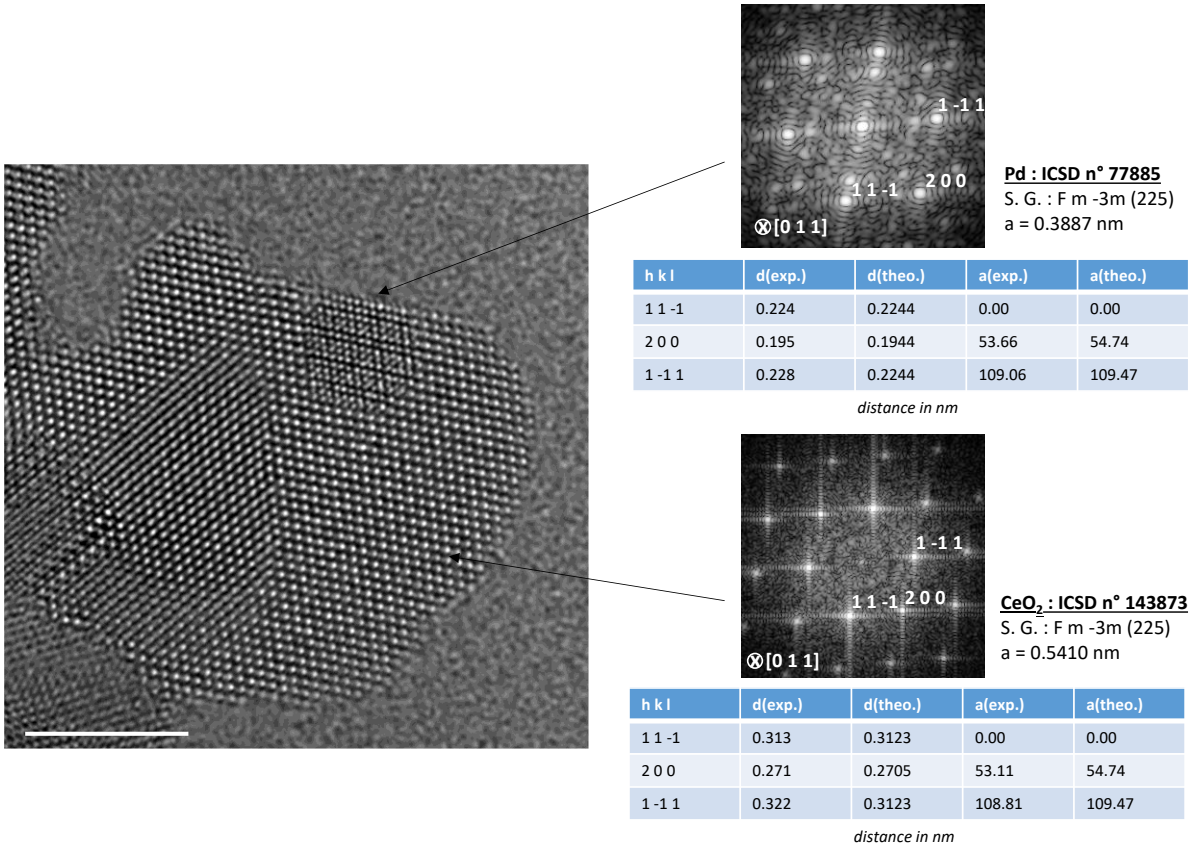

Figure S13. Left: STEM image of the 3 wt.% Pd/CeO_2-120 catalyst after *in situ* reduction at 500 °C for 2 h (18 mbar H_2). Right: Crystal structure of the resulting metallic Pd particles and of CeO_2 support as derived from the Fast Fourier Transform (FFT) diffractograms.

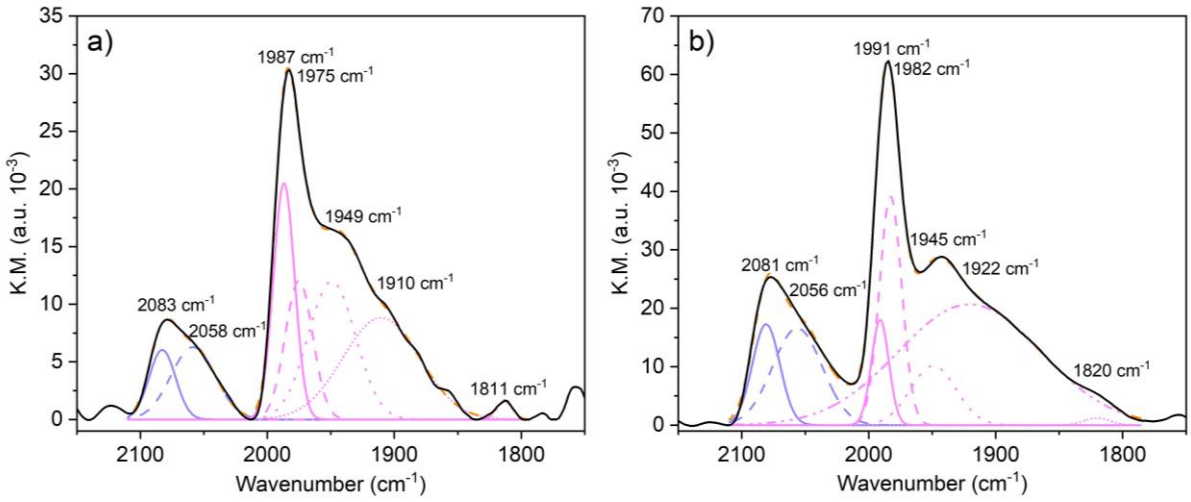

Figure S14. Results of DRIFTS measurements after CO adsorption at room temperature (1000 ppm CO/Ar) for the 1 wt.% Pd/CeO_2-120 catalyst (a) and the 3 wt.% Pd/CeO_2-120 catalyst (b) after CO reduction treatment at 500 °C for 1 h.

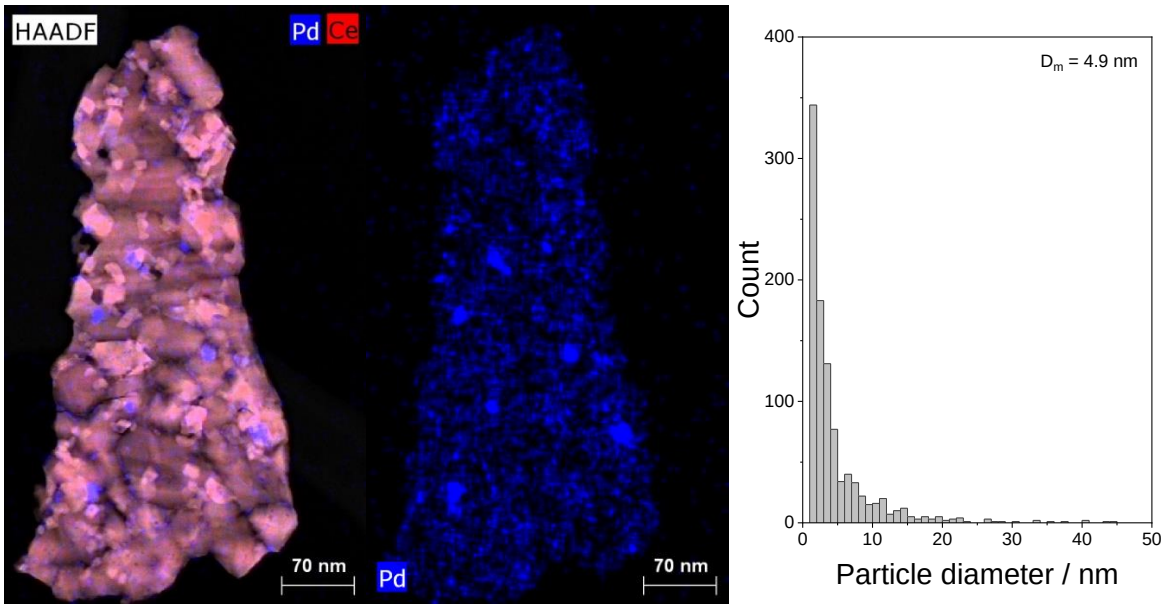

Figure S15. EDXS-map and the particle size distribution of 3 wt.% Pd/CeO_2-60 after calcination at 800 °C for 10 h in static air.

Table S1. Overview of catalyst composition determined by elemental analysis (ICP-OES) and surface area including pore volume from N_2 physisorption (BET).

	1Pd/CeO_2-120		2Pd/CeO_2-120		3Pd/CeO_2-120	
Elemental composition [wt.-%]	**Pd**	**Ce**	**Pd**	**Ce**	**Pd**	**Ce**
	0.90	74.6	1.91	73.6	2.93	72.5
Surface area [m^2/g]	116		127		106	
Pore volume [mL/g]	0.28		0.29		0.28	

Table S2. Temperatures for 10% (T_{10}), 50% (T_{50}) and 90% (T_{90}) CH_4 conversion during light-off over three catalysts with different loading supported on CeO_2 with surface area of 120 m^2/g after reductive treatment in either H_2 or CO at 500°C for 1h. The temperatures are reported for light-offs in dry (black) and wet (blue) methane oxidation feeds.

Activation treatment		**1st light-off**			**2nd light-off**			**3rd light-off**		
		T_{10}, °C	T_{50}, °C	T_{90}, °C	T_{10}, °C	T_{50}, °C	T_{90}, °C	T_{10}, °C	T_{50}, °C	T_{90}, °C
1Pd/CeO_2-120	H_2	242 (331)	283 (372)	315 (418)	439 (493)	-	-	480 (522)	-	-
	CO	249 (326)	287 (361)	321 (393)	289 (375)	337 (426)	394 (495)	306 (396)	366 (456)	439 (545)
2Pd/CeO_2-120	H_2	246 (332)	289 (378)	331 (451)	379 (448)	478 (550)	-	404 (477)	506	-
	CO	249 (327)	290 (361)	331 (393)	291 (376)	349 (426)	425 (495)	307 (395)	376 (456)	470 (545)
3Pd/CeO_2-120	H_2	249 (322)	292 (363)	338 (407)	317 (376)	396 (434)	500 (531)	324 (382)	410 (445)	519 (550)
	CO	256 (320)	300 (362)	353 (403)	302 (365)	373 (417)	470 (496)	312 (373)	392 (432)	501 (520)

Estimation of the monolayer fraction of Pd single sites (M_L(single site)) on ceria in substituted (110) nanopockets

The following equation was used:

$$\mathrm{M_L(single\ site)} = \frac{\mathrm{A_{UC}} * \mathrm{L} * \frac{\mathrm{N_A}}{\mathrm{M(Pd)}}}{\mathrm{A_{BET}}}$$

With:

Area of a unit cell:	$\mathrm{A_{UC}} = 4.25 * 10^{-19}\ \mathrm{m^2}$
Palladium loading:	$\mathrm{L} = 1 - 3\ \mathrm{wt.\%}$
Avogadro number:	$\mathrm{N}_A = 6.022 * 10^{23}\ \frac{1}{mol}$
Molar mass of palladium:	$\mathrm{M(Pt)} = 106.42\ \frac{g}{mol}$
CeO_2 - BET surface area	$\mathrm{A}_{BET} = 30 - 120\ \frac{m^2}{g}$

Accordingly, the following monolayer fractions were obtained for the different Pd/CeO_2 samples based on the ICP-OES analysis:

Table S3. Theoretical single site monolayer coverage for the different catalysts used in this study

Catalyst	BET surface area (m^2/g)	Single site monolayer coverage (%)
1PdCeO₂-120	120	20
2PdCeO₂-120	120	40
3PdCeO₂-120	120	60
2PdCeO₂-60	62	80
3PdCeO₂-60	62	120
2PdCeO₂-30	32	176

Calculation of reaction rates

Reaction rates were determined from the amount of methane (in mmol) converted per gram of Pd and per second (Table S4). Reaction rates at 300 °C were compared for different catalysts in Fig. 9. Since not all samples exhibited detectable conversions at this temperature, a linear regression based on the Arrhenius equation was used to calculate the reaction rates at 300 °C based on temperatures of four conversion points in the range of 5-20 % for each catalyst (see Fig. S16 and Tables S5-S12). For samples that did not reach 20 % conversion (1Pd/CeO_2-120 and 2Pd/CeO_2-120 after oxidation in 10 % O_2 at 800 °C), the conversion range of 2.5-10 % was used.

Table S4. Integral reaction rates calculated at 300 °C for catalysts with different Pd loadings and different surface areas of CeO_2, based on the light-off curves measured for methane oxidation or obtained by extrapolation. Additionally, the ratios between the rates of the 1st, 2nd and 3rd light-offs are reported.

Sample	Pd loading, wt. %	S_{BET}, m^2/g	Monolayer coverage, %	r_1 (1st LO), $mmol \cdot g_{Pd}^{-1} \cdot s^{-1}$	r_2 (2nd LO), $mmol \cdot g_{Pd}^{-1} \cdot s^{-1}$	r_3 (3rd LO), $mmol \cdot g_{Pd}^{-1} \cdot s^{-1}$	r_1/r_2	r_1/r_3
1Pd/CeO_2-120, red. CO	1	120	20	1.16	0.12	0.06	9.6	18.7
2Pd/CeO_2-120, red. CO	2	120	40	0.87	0.11	0.06	8.3	14.5
3Pd/CeO_2-120, red. CO	3	120	60	0.67	0.07	0.05	9.0	12.8
2Pd/CeO_2-60, red. CO	2	60	80	0.36	0.09	0.07	4.1	5.0
3Pd/CeO_2-60, red. CO	3	60	120	0.41	0.11	0.09	3.8	4.9
2Pd/CeO_2-30, red. CO	2	30	176	0.29	0.06	0.05	5.3	6.1
1Pd/CeO_2-120, red. H_2	1	120	20	1.04	$3 \cdot 10^{-3}$	$1 \cdot 10^{-3}$	365	1192
2Pd/CeO_2-120, red. H_2	2	120	40	0.73	0.01	$7 \cdot 10^{-3}$	59.6	105
2Pd/CeO_2-60, red. H_2	2	60	80	0.37	0.05	0.04	7.0	9.5
3Pd/CeO_2-120, red. H_2	3	120	60	0.85	0.05	0.04	18.2	23.9
3Pd/CeO_2-60, red. H_2	3	60	120	0.35	0.07	0.05	5.1	6.5
2Pd/CeO_2-30, red. H_2	2	30	176	0.28	0.05	0.04	6.1	6.9
2Pd/CeO_2-30 ox. 500 °C	2	30	176	0.10	0.06	-	1.5	-
2Pd/CeO_2-120, ox. 500 °C	2	120	40	0.02	$3 \cdot 10^{-3}$	$2 \cdot 10^{-3}$	4.6	6.9
1Pd/CeO_2-120, ox. 800 °C	1	120	20	$8 \cdot 10^{-5}$	-	-	-	-
2Pd/CeO_2-120, ox. 800 °C	2	120	40	$3 \cdot 10^{-4}$	-	-	-	-
3Pd/CeO_2-120, ox. 800 °C	3	120	80	$4 \cdot 10^{-4}$	-	-	-	-
2Pd/CeO_2-60, ox. 800 °C	2	60	60	0.04	-	-	-	-
3Pd/CeO_2-60, ox. 800 °C	3	60	120	0.05	-	-	-	-
2Pd/CeO_2-30, ox. 800 °C	2	30	176	0.03	0.02	0.02	1.4	1.5

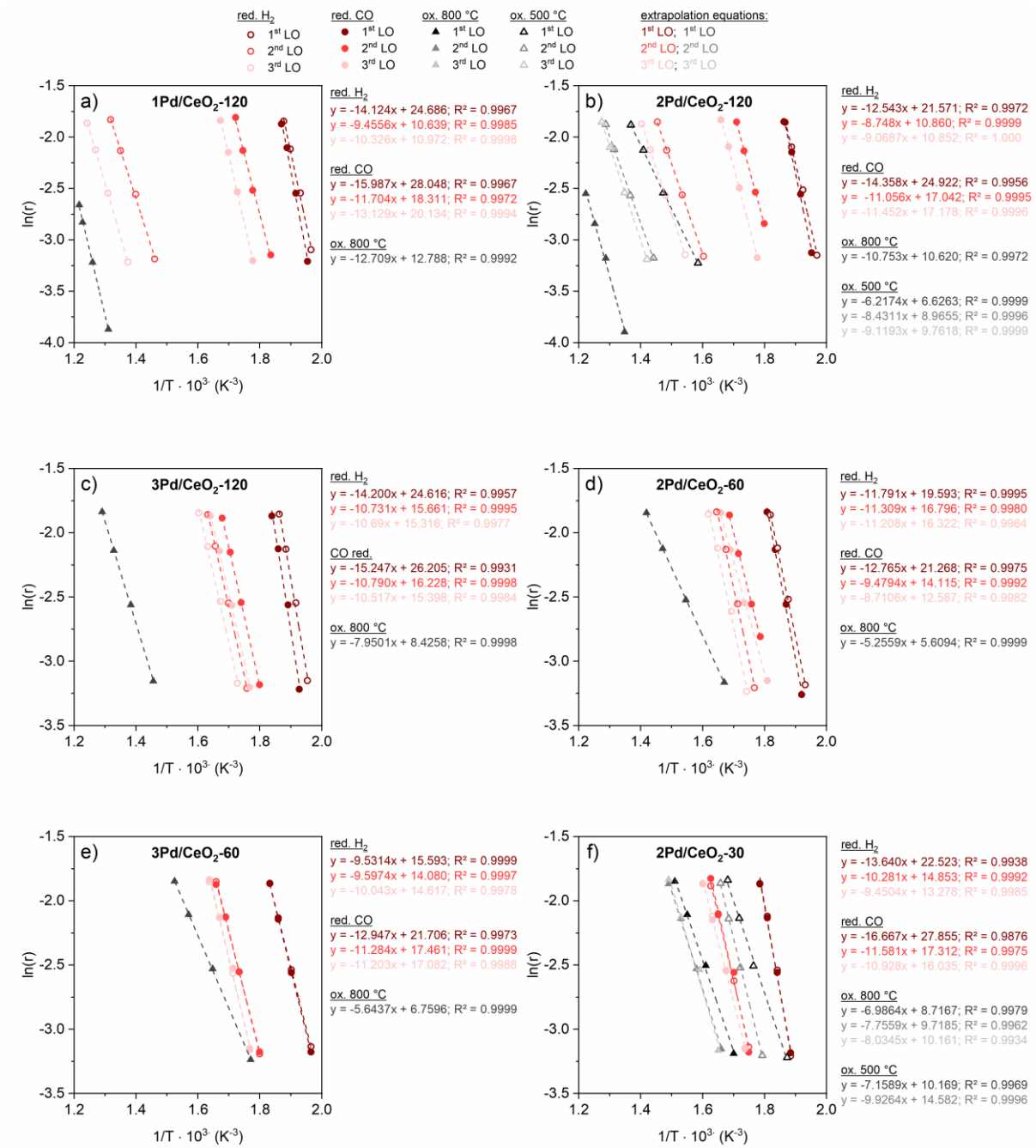

Figure S16. Arrhenius plots for the different Pd/CeO_2 catalysts investigated in this study after various treatments: reduction in 5 % H_2 (red. H_2); reduction in 0.5 % CO (red. CO); oxidation in 10 % O_2 at 500 °C and 800 °C (ox. 500 °C and ox 800 °C respectively). Gas mixture: 3200 ppm CH_4, 10 vol.% O_2 in N_2.

Table S5. Source data for Arrhenius diagrams reported in Fig. S16 for all samples after oxidative treatments in 10 % O_2 at 800 °C (ox. 800 °C).

Light-off	CH_4 conversion, %	T, °C	$T^{-1} \cdot 10^{-3}$, K^{-3}	r, mmol · g_{Pd}^{-1} · s^{-1}	ln(r)
	1Pd/CeO_2-120				
1st LO	2.6	490.0	1.31	0.021	-3.87
	5.1	520.9	1.26	0.040	-3.22
	7.5	541.9	1.23	0.059	-2.83
	8.8	548.9	1.22	0.070	-2.66
	Extrapolated	300.0	1.75	8.3E-5	-9.39
	2Pd/CeO_2-120				
1st LO	2.6	469.0	1.35	0.020	-3.89
	5.3	503.9	1.29	0.042	-3.18
	7.4	525.9	1.25	0.058	-2.84
	9.9	544.9	1.22	0.078	-2.55
	Extrapolated	300.0	1.75	2.9E-4	-8.15
	3Pd/CeO_2-120				
1st LO	5.4	413.9	1.46	0.043	-3.15
	9.7	450.0	1.39	0.077	-2.56
	14.9	480.0	1.33	0.118	-2.14
	20.1	502.0	1.29	0.160	-1.84
	Extrapolated	300.0	1.75	0.004	-5.45
	2Pd/CeO_2-60				
1st LO	5.3	325.9	1.67	0.042	-3.16
	10.1	373.9	1.55	0.080	-2.52
	15.1	406.9	1.47	0.120	-2.12
	20.0	431.9	1.42	0.158	-1.84
	Extrapolated	300.0	1.75	0.028	-3.56
	3Pd/CeO_2-60				
1st LO	5.0	291.9	1.77	0.039	-3.23
	10.1	334.1	1.65	0.080	-2.53
	15.3	364.0	1.57	0.122	-2.11
	19.9	383.0	1.52	0.158	-1.84
	Extrapolated	300.0	1.75	0.046	-3.09
	2Pd/CeO_2-30				
1st LO	5.2	314.9	1.7	0.041	-3.186
	10.3	348.0	1.61	0.082	-2.502
	15.4	371.9	1.55	0.122	-2.105
	19.9	390.0	1.51	0.158	-1.846
	Extrapolated	300.0	1.75	0.031	-3.476
2nd LO	5.4	330.9	1.66	0.043	-3.152
	10.1	358.0	1.58	0.08	-2.527
	14.9	380.9	1.53	0.118	-2.136
	19.5	397.9	1.49	0.155	-1.866
	Extrapolated	300.0	1.75	0.022	-3.817
3rd LO	5.3	331.9	1.65	0.042	-3.162
	10	356.9	1.59	0.079	-2.535
	15	380.0	1.53	0.119	-2.127
	20.2	398.9	1.49	0.16	-1.833
	Extrapolated	300.0	1.75	0.021	-3.861

Table S6. Source data for Arrhenius diagrams reported in Fig. S16 for 2Pd/CeO_2-120 and 2Pd/CeO_2-30 after oxidative treatments in 10 % O_2 at 500 °C (ox. 500 °C).

Light-off	CH_4 conversion, %	T, °C	$T^{-1} \cdot 10^{-3}$, K^{-3}	r, mmol · g_{Pd}^{-1} · s^{-1}	ln(r)
	2Pd/CeO_2-120				
1st LO	5.0	358.0	1.58	0.040	-3.22
	9.9	405.9	1.47	0.079	-2.54
	15.1	436.9	1.41	0.119	-2.12
	19.2	458.0	1.37	0.153	-1.88
	Extrapolated	300.0	1.75	0.015	-4.22
2nd LO	5.3	421.0	1.44	0.042	-3.18
	9.7	458.9	1.37	0.077	-2.57
	15.1	487.9	1.31	0.120	-2.12
	19.3	503.9	1.29	0.153	-1.88
	Extrapolated	300.0	1.75	0.003	-5.75
3rd LO	5.2	431.0	1.42	0.041	-3.19
	10.0	468.9	1.35	0.079	-2.54
	15.5	495.8	1.30	0.123	-2.10
	19.7	511.9	1.27	0.157	-1.85
	Extrapolated	300.0	1.75	0.002	-6.15
	2Pd/CeO_2-30				
1st LO	5.1	261.0	1.87	0.040	-3.22
	10.3	293.9	1.76	0.082	-2.50
	14.9	309.0	1.72	0.118	-2.13
	20.1	321.9	1.68	0.159	-1.84
	Extrapolated	300.0	1.75	0.098	-2.32
2nd LO	5.1	284.9	1.79	0.041	-3.20
	10.2	307.9	1.72	0.081	-2.52
	14.9	320.8	1.68	0.118	-2.14
	19.6	330.3	1.66	0.155	-1.86
	Extrapolated	300.0	1.75	0.065	-2.74

Table S7. Source data for Arrhenius diagrams reported in Fig. S16 for 1Pd/CeO_2-120 after reductive treatments.

Light-off	CH_4 conversion, %	T, °C	$T^{-1} \cdot 10^{-3}$, K^{-3}	r, mmol · g_{Pd}^{-1} · s^{-1}	ln(r)
	red. H_2				
1st LO	5.7	236.0	1.96	0.045	-3.09
	9.9	245.0	1.93	0.079	-2.54
	15.2	253.9	1.90	0.121	-2.11
	19.9	259.8	1.88	0.158	-1.84
	Extrapolated	300.0	1.75	1.036	0.04
2nd LO	5.2	411.9	1.46	0.041	-3.18
	9.8	441.9	1.40	0.078	-2.55
	15.0	467.9	1.35	0.119	-2.13
	20.2	486.0	1.32	0.161	-1.83
	Extrapolated	300.0	1.75	0.003	-5.86
3rd LO	5.1	455.0	1.37	0.040	-3.21
	9.9	490.9	1.31	0.079	-2.54
	15.1	514.9	1.27	0.120	-2.12
	19.6	532.0	1.24	0.155	-1.86
	Extrapolated	300.0	1.75	0.001	-7.05
	red. CO				
1st LO	5.1	238.9	1.95	0.040	-3.21
	9.9	249.0	1.92	0.079	-2.54
	15.4	256.9	1.89	0.122	-2.10
	19.4	261.9	1.87	0.154	-1.87
	Extrapolated	300.0	1.75	1.159	0.15
2nd LO	5.4	272.0	1.83	0.043	-3.14
	10.2	289.9	1.78	0.081	-2.52
	15.0	300.0	1.75	0.119	-2.13
	20.7	307.9	1.72	0.164	-1.81
	Extrapolated	300.0	1.75	0.121	-2.11
3rd LO	5.1	289.9	1.78	0.041	-3.20
	10.0	305.9	1.73	0.080	-2.53
	14.7	316.0	1.70	0.117	-2.15
	20.1	325.0	1.67	0.159	-1.84
	Extrapolated	300.0	1.75	0.062	-2.78

Table S8. Source data for Arrhenius diagrams reported in Fig. S16 for 2Pd/CeO_2-120 after reductive treatments.

Light-off	CH_4 conversion, %	T, °C	$T^{-1} \cdot 10^{-3}$, K^{-3}	r, mmol · g_{Pd}^{-1} · s^{-1}	ln(r)
	red. H_2				
1st LO	5.4	234.9	1.97	0.043	-3.15
	10.2	247.0	1.92	0.081	-2.51
	15.5	257.0	1.89	0.123	-2.09
	19.7	262.9	1.87	0.157	-1.85
	Extrapolated	300.0	1.75	0.727	-0.32
2nd LO	5.4	351.0	1.60	0.043	-3.16
	9.7	379.0	1.53	0.077	-2.56
	15.0	401.0	1.48	0.119	-2.13
	19.8	414.9	1.45	0.157	-1.85
	Extrapolated	300.0	1.75	0.012	-4.41
3rd LO	5.4	375.0	1.54	0.043	-3.14
	9.7	403.0	1.48	0.077	-2.57
	15.1	426.0	1.43	0.120	-2.12
	19.4	439.9	1.40	0.154	-1.87
	Extrapolated	300.0	1.75	0.007	-4.98
	red. CO				
1st LO	5.5	239.5	1.95	0.044	-3.12
	9.8	248.9	1.92	0.078	-2.55
	14.8	256.9	1.89	0.117	-2.14
	19.8	264.0	1.86	0.157	-1.85
	Extrapolated	300.0	1.75	0.874	-0.13
2nd LO	7.4	282.9	1.80	0.058	-2.84
	10.0	291.9	1.77	0.079	-2.53
	14.9	303.9	1.73	0.119	-2.13
	19.8	311.9	1.71	0.157	-1.85
	Extrapolated	300.0	1.75	0.105	-2.25
3rd LO	5.3	289.9	1.78	0.042	-3.17
	10.4	308.9	1.72	0.083	-2.49
	15.6	320.9	1.68	0.124	-2.09
	20.3	330.0	1.66	0.161	-1.83
	Extrapolated	300.0	1.75	0.060	-2.81

Table S9. Source data for Arrhenius diagrams reported in Fig. S16 for 3Pd/CeO_2-120 after reductive treatments.

Light-off	CH_4 conversion, %	T, °C	$T^{-1} \cdot 10^{-3}$, K^{-3}	r, mmol · g_{Pd}^{-1} · s^{-1}	ln(r)
	red. H_2				
1st LO	5.4	239.0	1.95	0.043	-3.15
	9.9	248.9	1.92	0.079	-2.54
	15.0	257.9	1.88	0.119	-2.13
	19.8	264.0	1.86	0.157	-1.85
	Extrapolated	300.0	1.75	0.847	-0.17
2nd LO	5.1	295.9	1.76	0.040	-3.21
	9.9	315.9	1.70	0.079	-2.54
	15.4	330.9	1.66	0.122	-2.10
	19.7	340.0	1.63	0.156	-1.86
	Extrapolated	300.0	1.75	0.047	-3.07
3rd LO	5.3	306.0	1.73	0.042	-3.17
	10.0	324.9	1.67	0.079	-2.53
	15.3	339.9	1.63	0.122	-2.11
	19.9	351.0	1.60	0.158	-1.84
	Extrapolated	300.0	1.75	0.035	-3.34
	red. CO				
1st LO	5.1	246.0	1.93	0.040	-3.22
	9.8	256.0	1.89	0.077	-2.56
	15.1	264.9	1.86	0.120	-2.12
	19.5	270.9	1.84	0.155	-1.87
	Extrapolated	300.0	1.75	0.667	-0.40
2nd LO	5.2	283.0	1.80	0.042	-3.18
	9.9	302.0	1.74	0.079	-2.54
	14.7	313.8	1.70	0.117	-2.15
	19.2	323.0	1.68	0.152	-1.88
	Extrapolated	300.0	1.75	0.074	-2.60
3rd LO	5.1	292.9	1.77	0.041	-3.20
	9.7	311.9	1.71	0.077	-2.56
	14.8	326.0	1.67	0.118	-2.14
	19.5	337.0	1.64	0.155	-1.87
	Extrapolated	300.0	1.75	0.052	-2.96

Table S10. Source data for Arrhenius diagrams reported in Fig. S16 for 2Pd/CeO_2-60 after reductive treatments.

Light-off	CH_4 conversion, %	T, °C	$T^{-1} \cdot 10^{-3}$, K^{-3}	r, mmol · g_{Pd}^{-1} · s^{-1}	ln(r)
	red. H_2				
1st LO	5.2	245.0	1.93	0.042	-3.18
	10.2	260.0	1.88	0.081	-2.52
	15.2	270.0	1.84	0.120	-2.12
	19.7	277.0	1.82	0.156	-1.86
	Extrapolated	300.0	1.75	0.373	-0.99
2nd LO	5.1	292.0	1.77	0.041	-3.20
	9.8	310.9	1.71	0.078	-2.55
	15.0	323.9	1.68	0.119	-2.13
	20.1	334.9	1.64	0.159	-1.84
	Extrapolated	300.0	1.75	0.054	-2.92
3rd LO	5.0	301.0	1.74	0.039	-3.23
	9.2	317.0	1.69	0.074	-2.61
	15.2	333.9	1.65	0.120	-2.12
	19.8	344.9	1.62	0.157	-1.85
	Extrapolated	300.0	1.75	0.039	-3.24
	red. CO				
1st LO	4.8	248.0	1.92	0.038	-3.26
	9.8	262.0	1.87	0.078	-2.56
	15.0	272.2	1.83	0.119	-2.13
	20.1	280.2	1.81	0.159	-1.84
	Extrapolated	300.0	1.75	0.364	-1.01
2nd LO	7.6	286.9	1.79	0.060	-2.81
	9.8	295.9	1.76	0.078	-2.55
	14.5	309.9	1.72	0.115	-2.16
	19.6	320.0	1.69	0.156	-1.86
	Extrapolated	300.0	1.75	0.088	-2.43
3rd LO	5.4	280.0	1.81	0.043	-3.15
	9.9	304.0	1.73	0.079	-2.54
	15.0	318.8	1.69	0.119	-2.13
	20.0	330.0	1.66	0.158	-1.84
	Extrapolated	300.0	1.75	0.073	-2.61

Table S11. Source data for Arrhenius diagrams reported in Fig. S16 for 3Pd/CeO_2-60 after reductive treatments.

Light-off	CH_4 conversion, %	T, °C	$T^{-1} \cdot 10^{-3}$, K^{-3}	r, mmol · g_{Pd}^{-1} · s^{-1}	ln(r)
	red. H_2				
1st LO	5.5	236.0	1.96	0.044	-3.13
	10.0	252.9	1.90	0.079	-2.53
	15.0	264.9	1.86	0.119	-2.13
	19.6	272.9	1.83	0.155	-1.86
	Extrapolated	300.0	1.75	0.353	-1.04
2nd LO	5.2	282.9	1.80	0.041	-3.19
	9.8	304.0	1.73	0.078	-2.55
	15.1	318.9	1.69	0.120	-2.12
	19.8	330.0	1.66	0.158	-1.85
	Extrapolated	300.0	1.75	0.069	-2.67
3rd LO	5.4	293.0	1.77	0.043	-3.15
	9.7	311.0	1.71	0.077	-2.56
	15.0	325.9	1.67	0.119	-2.13
	19.8	337.9	1.64	0.157	-1.85
	Extrapolated	300.0	1.75	0.054	-2.91
	red. CO				
1st LO	5.3	247.9	1.92	0.042	-3.17
	9.8	259.8	1.88	0.078	-2.56
	14.8	269.7	1.84	0.118	-2.14
	19.6	276.9	1.82	0.156	-1.86
	Extrapolated	300.0	1.75	0.411	-0.89
2nd LO	5.3	273.9	1.83	0.042	-3.17
	9.8	290.9	1.77	0.078	-2.55
	15.0	302.9	1.74	0.119	-2.13
	19.4	310.9	1.71	0.154	-1.87
	Extrapolated	300.0	1.75	0.107	-2.23
3rd LO	5.4	281.0	1.81	0.043	-3.16
	10.1	297.9	1.75	0.080	-2.52
	15.0	309.9	1.72	0.119	-2.13
	20.2	319.9	1.69	0.160	-1.83
	Extrapolated	300.0	1.75	0.085	-2.47

Table S12. Source data for Arrhenius diagrams reported in Fig. S16 for 2Pd/CeO_2-30 after reductive treatments.

Light-off	CH_4 conversion, %	T, °C	$T^{-1} \cdot 10^{-3}$, K^{-3}	r, mmol · g_{Pd}^{-1} · s^{-1}	ln(r)
	red. H_2				
1st LO	5.1	257.9	1.88	0.041	-3.21
	10.0	270.3	1.84	0.079	-2.54
	15.2	279.9	1.81	0.120	-2.12
	19.6	287.4	1.78	0.155	-1.86
	Extrapolated	300.0	1.75	0.277	-1.28
2nd LO	5.5	298.9	1.75	0.044	-3.13
	9.2	314.9	1.70	0.073	-2.62
	15.5	333.0	1.65	0.123	-2.10
	19.2	342.0	1.63	0.152	-1.88
	Extrapolated	300.0	1.75	0.046	-3.09
3rd LO	5.4	302.9	1.74	0.043	-3.14
	9.9	323.9	1.68	0.079	-2.54
	15.2	340.0	1.63	0.120	-2.12
	19.5	352.0	1.60	0.155	-1.87
	Extrapolated	300.0	1.75	0.040	-3.21
	red. CO				
1st LO	5.2	264.9	1.86	0.042	-3.18
	9.8	274.0	1.83	0.078	-2.55
	15.0	282.0	1.80	0.119	-2.13
	19.5	288.9	1.78	0.155	-1.87
	Extrapolated	300.0	1.75	0.291	-1.23
2nd LO	5.3	292.9	1.77	0.042	-3.18
	9.8	308.9	1.72	0.078	-2.55
	15.4	323.0	1.68	0.122	-2.11
	20.4	333.0	1.65	0.161	-1.82
	Extrapolated	300.0	1.75	0.055	-2.90
3rd LO	5.4	296.9	1.75	0.043	-3.15
	10.0	314.9	1.70	0.079	-2.54
	14.8	328.0	1.66	0.117	-2.15
	19.6	338.0	1.64	0.155	-1.86
	Extrapolated	300.0	1.75	0.048	-3.04

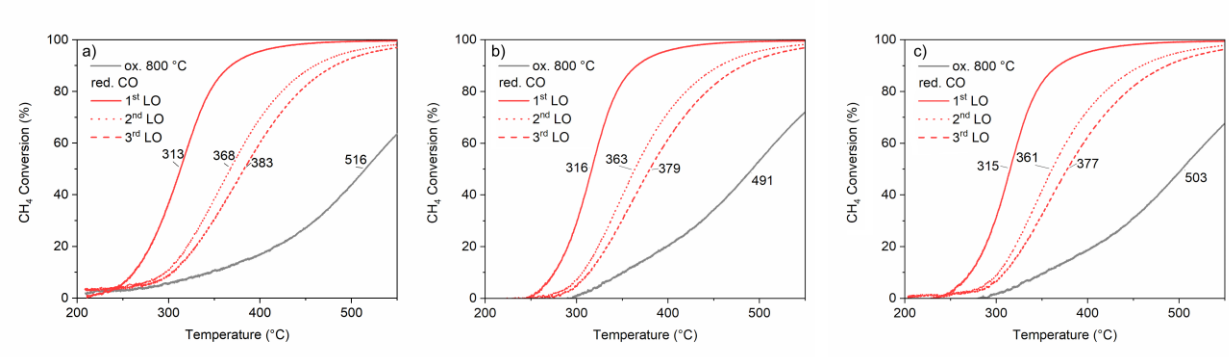

Figure S17. Conversion of methane by total oxidation during 3 consecutive light-offs for 2Pd/CeO_2-60 catalyst after thermal treatment at 800 °C in air (1 h at 800 °C in 10 % O_2) followed by a light-off and subsequent reduction (1 h at 500 °C in 0.5 % CO) followed by 3 light offs. Panels a, b, and c correspond to the first, second and third cycles, respectively. Gas mixture: 3200 ppm CH_4, 10 vol.% O_2 in N_2. The temperature of 50 % CH_4 conversion is indicated next to each conversion curve.

Details on the density functional theory calculations

CO adsorption models

Four different types of models were considered for the calculation of vibrational frequencies: single atoms, small clusters (dimers and trimers), nanoparticles, and extended Pd surfaces. For nanoparticles and extended Pd surfaces, a high CO coverage was considered, to allow for the adsorption of CO on a wider variety of sites. The results of the vibrational analysis are summarized in Table S5.

Single atoms

PdO_x species were adsorbed on a 9-layer supercell of $CeO_2(111)$ cleaved from the ceria bulk with the equilibrium lattice constant of 5.455 Å. The atoms in the 3 bottom atomic layers were kept frozen in their bulk positions. Pd/CeO_2 consist of two Pd atoms adsorbed on the same (2×2) cell, with one CO molecule on each of them (Figure S17a), whereas PdO/CeO_2 and PdO_2/CeO_2 have only one Pd atom and one CO molecule per supercell of (2×2) and (3×3), respectively, to avoid lateral interactions with periodic replica (Figures S17b–S17d).

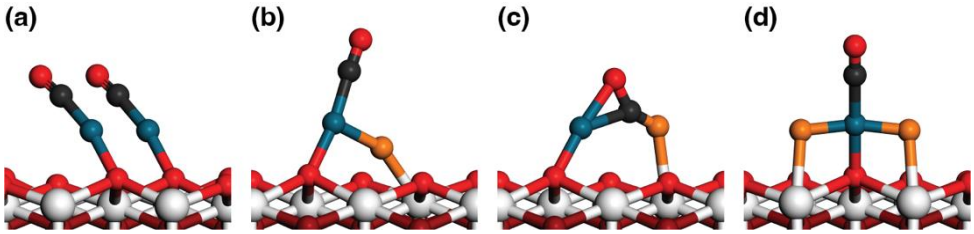

Figure S18. DFT-optimized structures of CO adsorbed on single atom systems. (a) $Pd/CeO_2(111)$. (b) $PdO/CeO_2(111)$, CO on Pd. (c) $PdO/CeO_2(111)$, CO on O forming a CO_2 species. (d) $PdO_2/CeO_2(111)$. Ce in gray, C in black, O from the surface and from CO in red, subsurface O in dark red, and excess O in orange.

Small clusters

Pd_2 and Pd_3 clusters were adsorbed on a 9-layer (3×3) supercell of $CeO_2(111)$ (Figure S18). Two CO molecules must be adsorbed on the Pd_2 cluster to stabilize linear adsorption (Figure S18a). For the cases labeled as CO_2 (Figures S18c and S18f) there is an additional oxygen atom over the stoichiometric amount, or in other words, these cases correspond to CO adsorbed on Pd_2O and Pd_3O clusters, respectively.

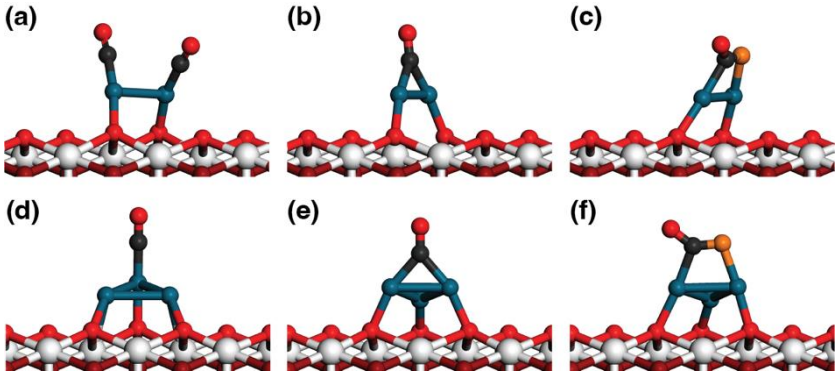

Figure S19. DFT-optimized structures of CO adsorbed on small Pd clusters. $Pd_2/CeO_2(111)$: (a) linear, (b) bridge, (c) forming CO_2. $Pd_3/CeO_2(111)$: (d) linear, (e) bridge, (f) forming CO_2.

Nanoparticles

The most stable high-symmetry isomer of Pd_{147} in gas phase, namely a strongly irregular truncated octahedron, was selected as a model of small nanoparticles (~1.5 nm). High CO coverage models were obtained by starting from 1 ML (1 CO per surface Pd atom) and removing a fraction of the CO molecules to obtain a coverage of 0.75 ML. Several random configurations were generated in this way, and the one with the lowest energy was further improved via ab initio molecular dynamics using canonical sampling through a velocity rescaling thermostat at 1000 K.[1] These calculations were run with the CP2K code, with a Double-ζ Gaussian basis set and an auxiliary plane wave basis (GPW approach).[2, 3] Low energy structures were quenched to 0 K with VASP and compared with the randomly generated initial structure. The lowest energy structure was then adsorbed on a 6-layer (6×6) supercell of $CeO_2(111)$ (Figure S19).

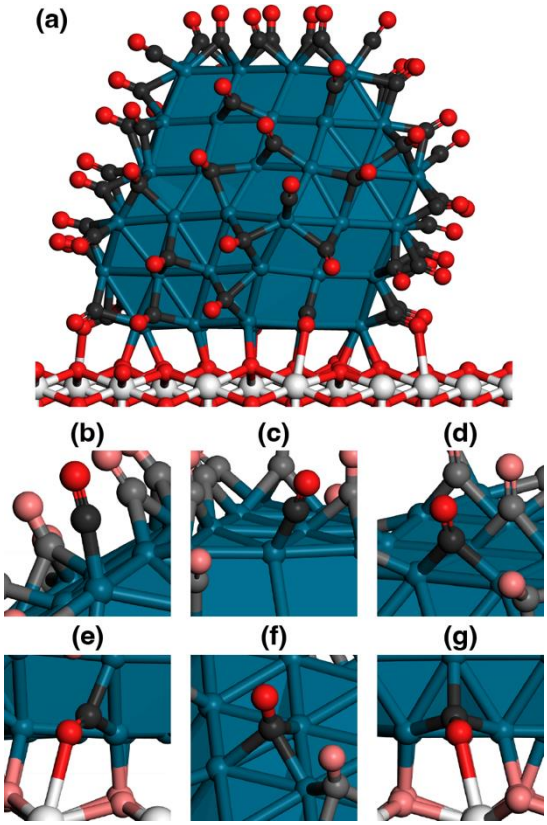

Figure S20. (a) DFT-optimized structure of the Pd_{147} nanoparticle covered by 0.75 ML of CO and adsorbed on CeO_2(111). CO adsorption sites highlighted: (b) Linear at vertex, (c) Linear on edge, (d) bridge on edge, (e) bridge at the interface, (f) 3-fold on facet, (g) 3-fold at the interface. Neighboring CO and surface oxygen are represented in lighter colors, to emphasize the representative CO molecule.

Extended Pd surfaces

The Pd and PdO surface slabs were cleaved from the corresponding bulks. The optimized equilibrium lattice constant of bulk Pd was a = 3.888 Å, whereas those of bulk PdO were a = 3.066 Å and c = 5.367 Å. A 5-layer slab was used for Pd(111), 4-layer for Pd(100), and 9-layer for PdO(101).

Adsorption of CO on Pd(111) is most favorable on 3-fold fcc sites, but linear and 3-fold CO can coexist at a high coverage of 0.75 ML (Figure S20a). Regarding the adsorption of CO_2, the saturation coverage is 0.33 ML (Figure S20b), with higher coverage resulting in CO_2 desorption.

On the Pd(100) surface, CO_2 adopts a bridge configuration, even at a high coverage of 0.75 ML (Figure S20c). For CO2, a coverage of 0.50 ML was evaluated (Figure S20d).

Finally, the linear adsorption of CO on a Pd oxide surface, namely PdO(101), was considered as well (Figure S20e).

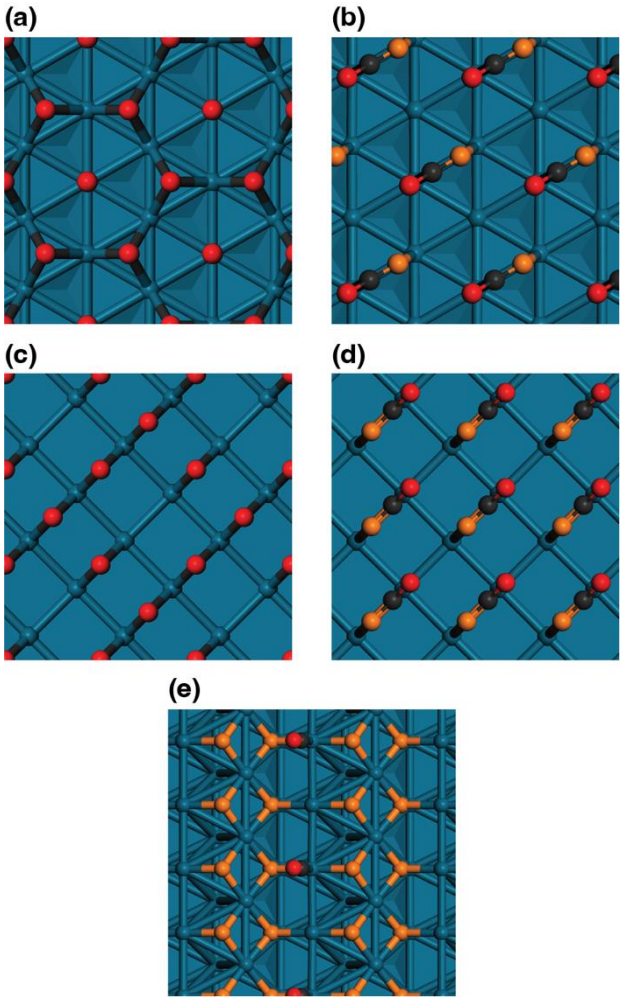

Figure S21. DFT-optimized structures of CO high-coverage adsorption on Pd surfaces. (a) CO on Pd(111), (b) CO_2 on Pd(111), (c) CO on Pd(100), (d) CO_2 on Pd(100). (e) Structure of CO adsorption on a PdO(101).

Table S12. DFT-calculated adsorption energies and stretching frequencies of CO. For the systems with more than one CO molecule in the calculation cell, the adsorption energy corresponds to the opposite of the desorption energy of a CO molecule from the corresponding adsorption site.

System	CO adsorption	Figure	Adsorption energy, eV	Frequency, cm^{-1}
	Gas-phase		0	2143
$Pd/CeO_2(111)$	Linear	S18a	−2.48	2078
$PdO/CeO_2(111)$	Linear on Pd	S18b	−1.04	2083
	Linear on O	S18c	−3.82	1924
$PdO_2/CeO_2(111)$	Linear on Pd	S18d	−1.34	2131
$Pd_2/CeO_2(111)$	Linear	S19a	−1.59	2075
	Bridge	S19b	−3.01	1880
	CO_2	S19c	−2.89	1768
$Pd_3/CeO_2(111)$	Linear	S19d	−2.83	2062
	Bridge	S19e	−3.23	1875
	CO_2	S19f	−2.11	1756
$Pd_{147}/CeO_2(111)$	Linear on vertex	S20b	−1.52	2064
	Linear on edge	S20c	−1.23	2043
	Bridge on edge	S20d	−1.78	1969
	Bridge at the interface	S20e	−1.50	1802
	3-fold on facet	S20f	−1.74	1845
	3-fold at the interface	S20g	−1.87	1706
Pd(111)	0.75 ML CO linear vib mode	S21a	−1.26	2106
	0.75 ML CO 3-fold vib mode	S21a	−1.55	1897
	0.33 ML CO_2	S21b	−2.28	1923
Pd(100)	0.75 ML CO bridge	S21c	−1.82	2028
	0.50 ML CO_2	S21d	−2.21	1978
PdO(101)	Linear on Pd	S21e	−1.69	2104

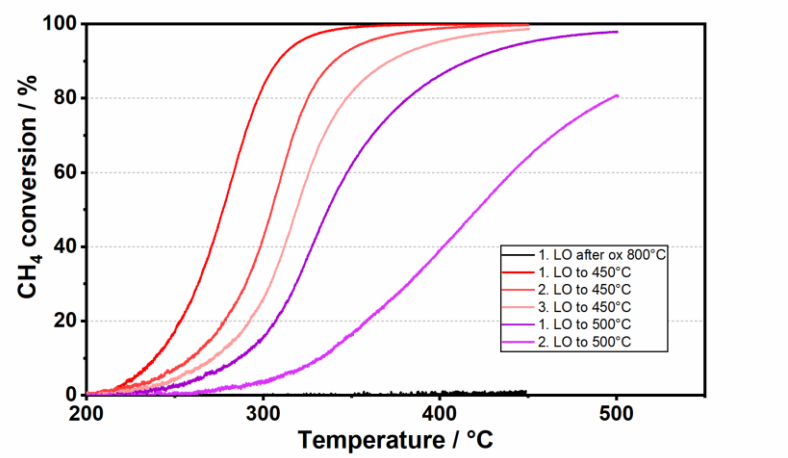

Figure S22. Total oxidation of methane: consecutive light-offs to 450 °C and 500 °C respectively for 1 wt.% Pd/CeO_2-120 after oxidation at 800 °C for 1 h and reduction for 60 min in 2 % H_2/N_2 at 500 °C. Gas mixture: 3200 ppm CH_4, 10 vol.% O_2 in N_2 at a weight hourly space velocity of 20000 $L \cdot g_{NM}^{-1} \cdot h^{-1}$.

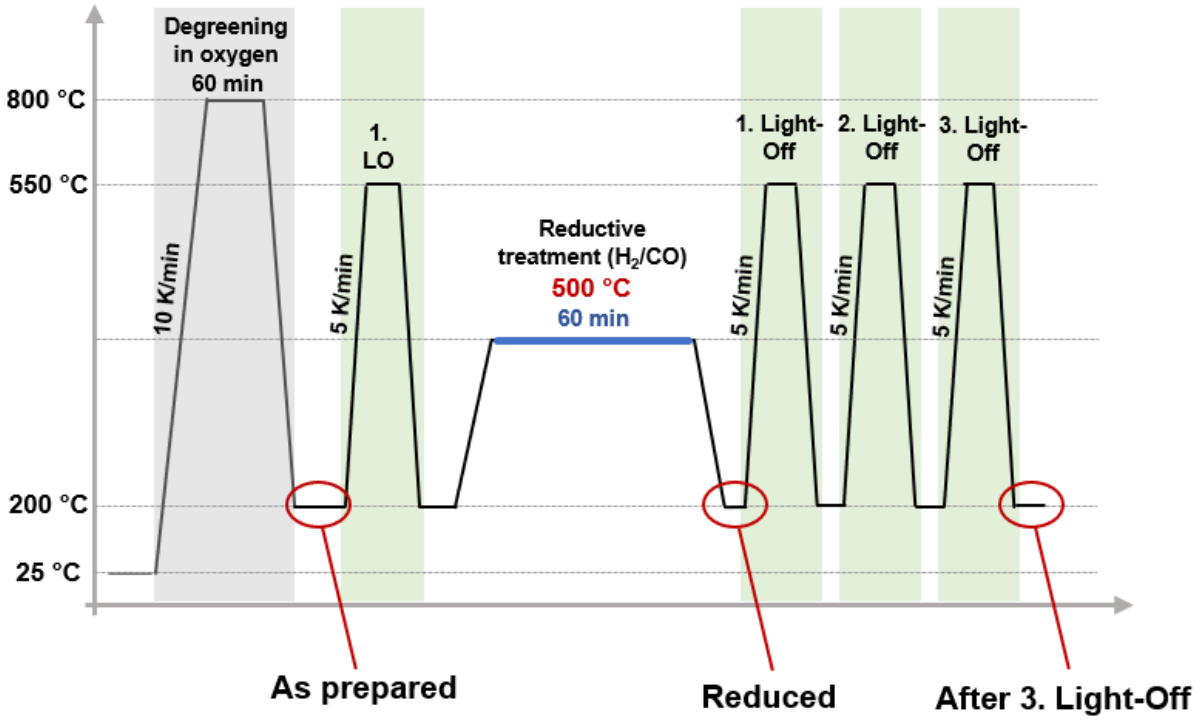

Figure S23. General procedure for catalytic activity tests, operando XAS measurements and sample pre-treatment for ex-situ characterization. Red circles mark the different catalyst states.

References

[1] G. Bussi, D. Donadio, M. Parrinello, Canonical sampling through velocity rescaling, J. Chem. Phys., 126 (2007).
[2] J. Hutter, M. Iannuzzi, F. Schiffmann, J. VandeVondele, cp2k: atomistic simulations of condensed matter systems, Wiley Interdisciplinary Reviews: Computational Molecular Science, 4 (2014) 15-25.
[3] B.G. Lippert, J.H. PARRINELLO, MICHELE, A hybrid Gaussian and plane wave density functional scheme, Molecular Physics, 92 (1997) 477-488.